ADVANCED MATERIALS

Supporting Information

for *Adv. Mater.,* DOI: 10.1002/adma.202200512

Multiphoton Lithography of Organic Semiconductor Devices for 3D Printing of Flexible Electronic Circuits, Biosensors, and Bioelectronics

*Omid Dadras-Toussi, Milad Khorrami, Anto Sam Crosslee Louis Sam Titus, Sheereen Majd, Chandra Mohan, and Mohammad Reza Abidian**

Supporting Information

Multiphoton Lithography of Organic Semiconductor Devices for 3D Printing of Flexible Electronic Circuits, Biosensors, and Bioelectronics

Omid Dadras-Toussi, Milad Khorrami, Anto Sam Crosslee Louis Sam Titus, Sheereen Majd, Chandra Mohan, and Mohammad Reza Abidian[*]

Effect of DMSO Concentration in the Resin on MPL-fabricated Microstructures

As shown in **Figure S1A**, OS would aggregate in the resin without DMSO, which demonstrates its vital role in preparation of homogeneous resin for MPL. Microstructures fabricated from OS composite resins with DMSO concentrations higher than 35 wt% did not have mechanical integrity and tend to detach from the substrate (**Figures S1B-D**). While the OS composite resin with DMSO concentration range between 25 wt% and 35 wt% was printable (**Figure S1E**), the OS composite resins were not MPL-compatible with DMSO concentrations higher than 45 wt%.

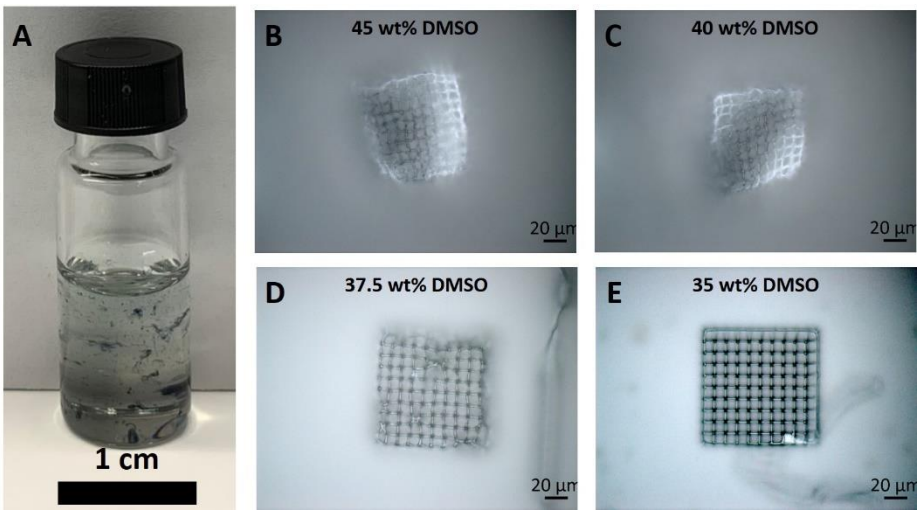

Figure S1. Role of DMSO in the resin formulation: A) Aggregation of OS in resin without DMSO, and upright micrograph of MPL-fabricated structures using resins with B) 45 wt% DMSO, C) 40 wt% DMSO, D) 37.5 wt% DMSO, and E) 35 wt% DMSO.

Resin stability and homogeneity

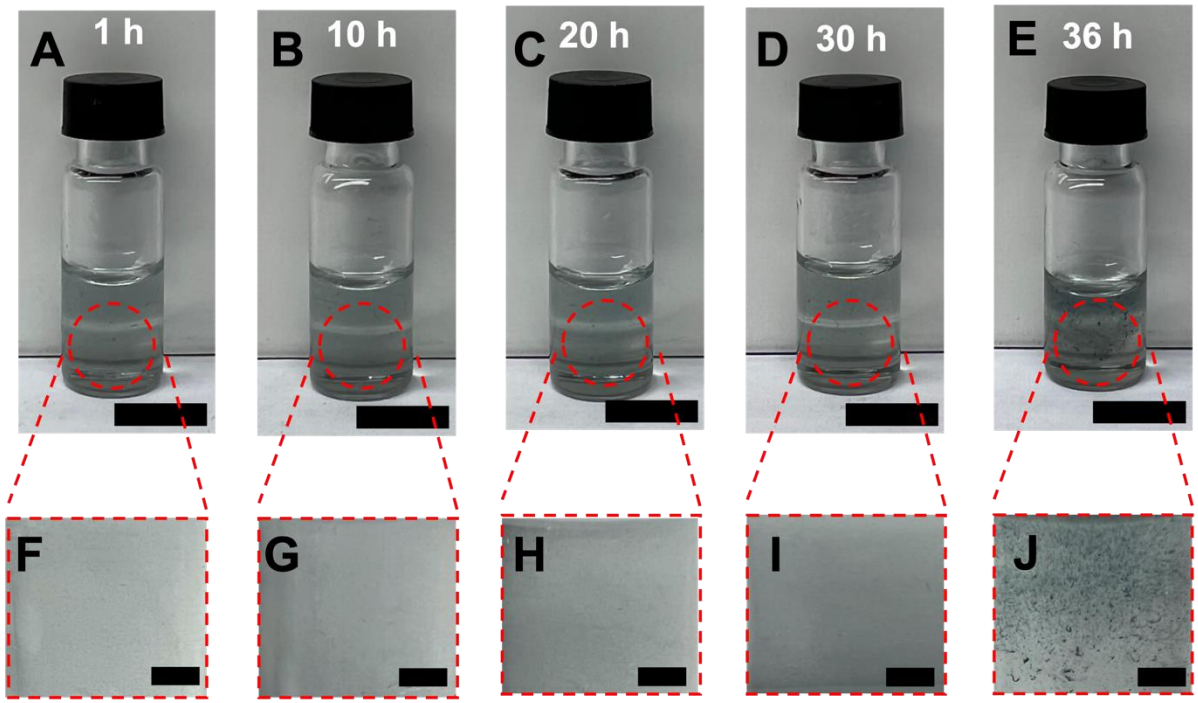

Figure S2. Resin stability and homogeneity: A-E) optical micrographs of resin stability over time at 1 h, 10 h, 20 h, 30 h, and 36 h after preparation scale bars: 1 cm). F-J) higher magnification optical micrographs of A-E, (scale bar: 1mm).

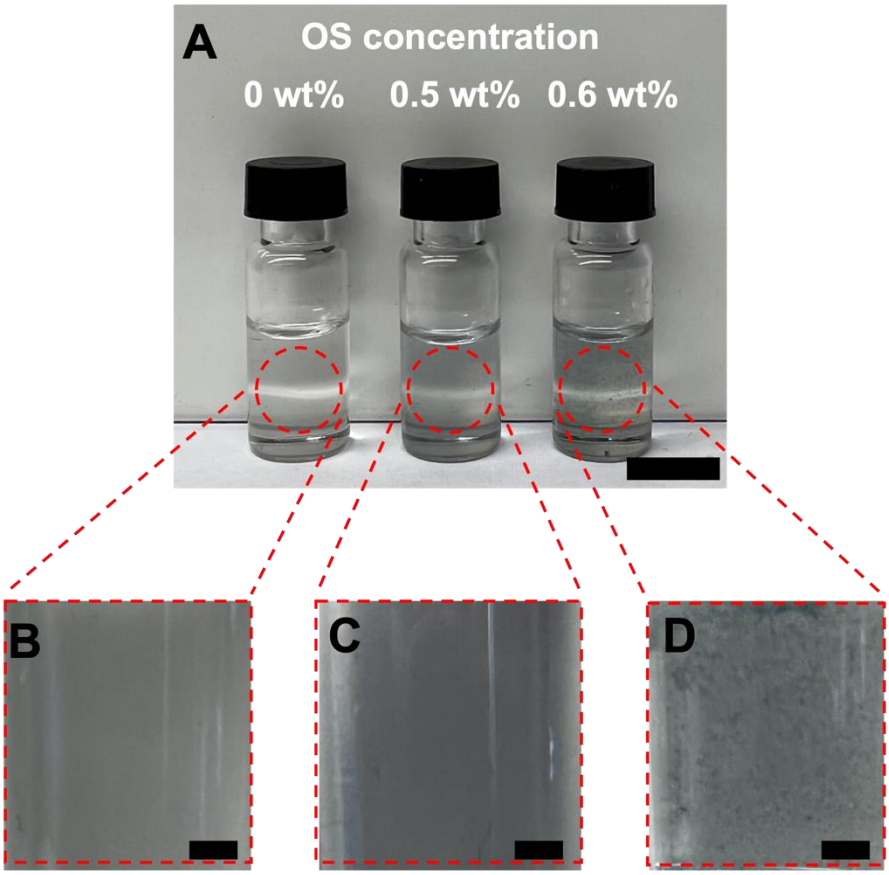

Figure S3. Effect of OS concentration on resin homogeneity. (Scale bar is 10 mm in A and 1mm in B-D).

SEM micrographs of 3D microstructures

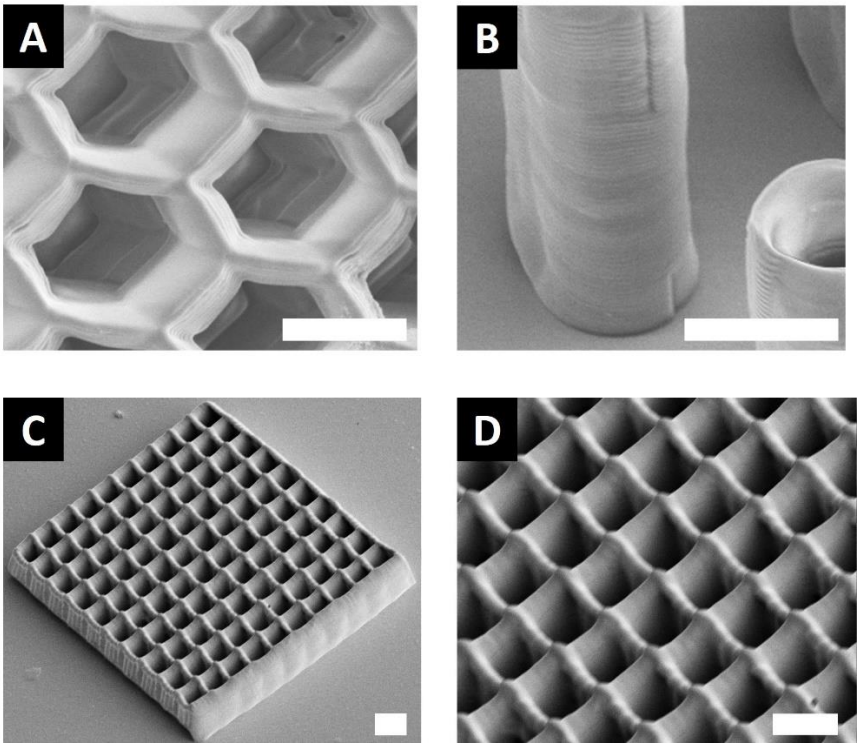

Figure S4. Higher SEM micrographs of micro-honeycomb (A), higher SEM micrographs vertical micro-tubes (B), micro-grid (C), and the center of the micro-grid (D) (scale bars: 10 µm).

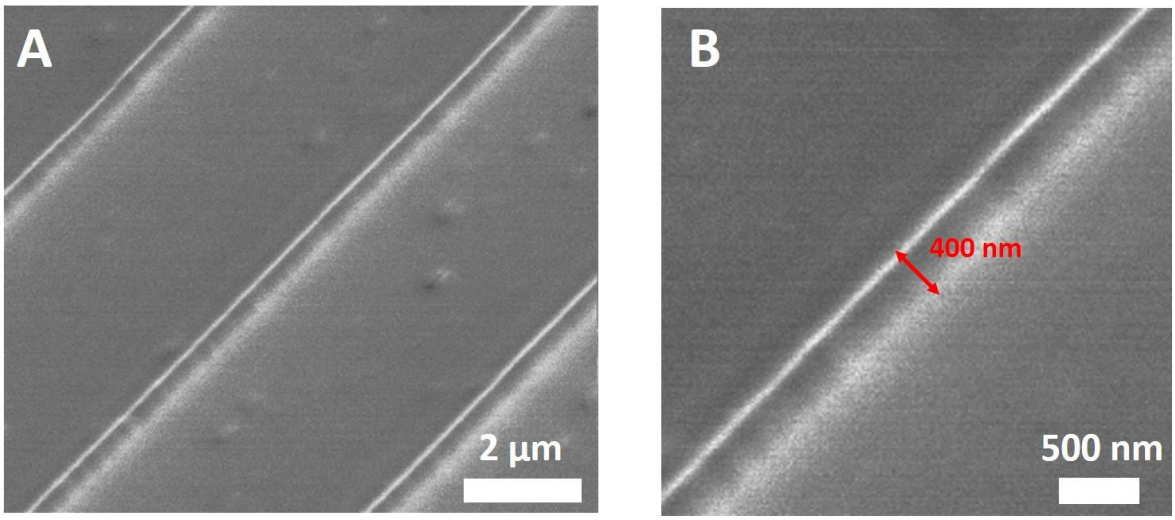

Figure S5. A and B) SEM of MPL-fabricated lines using an oil immersion objective lens 63X (NA 1.4), with laser power of 28 mW and focused scan speed of 100 µm s^{-1}.

Effect of OS Content on conductivity of MPL-Fabricated Microstructures

To measure the electrical conductivity, first, a partially Au-coated coverslip was fabricated (see Fabrication of gold-coated substrates in the Experimental Section). Resins with various OS concentrations were prepared (i.e. 0 wt% (C0), 0.1 wt% (C1), 0.2 wt% (C2), 0.3 wt% (C3), 0.4 wt% (C4), and 0.5 wt% (C5)). Bar-shaped microstructures connected two gold-coated parts via MPL process (**Figure S6A**). Current-voltage (I-V) measurement was performed (**Figure S6B**), and electrical conductivity was calculated based on the following equation:

$$\sigma = \frac{G\,A}{l} \qquad \text{(Equation S1)}$$

, where σ is electrical conductivity (S m^{-1}), G is electrical conductance (S) and is derived from the slope of I-V curve, A is the cross-section area of the microstructure (10 µm × 10 µm) and l is the length of the microstructure (265 µm).

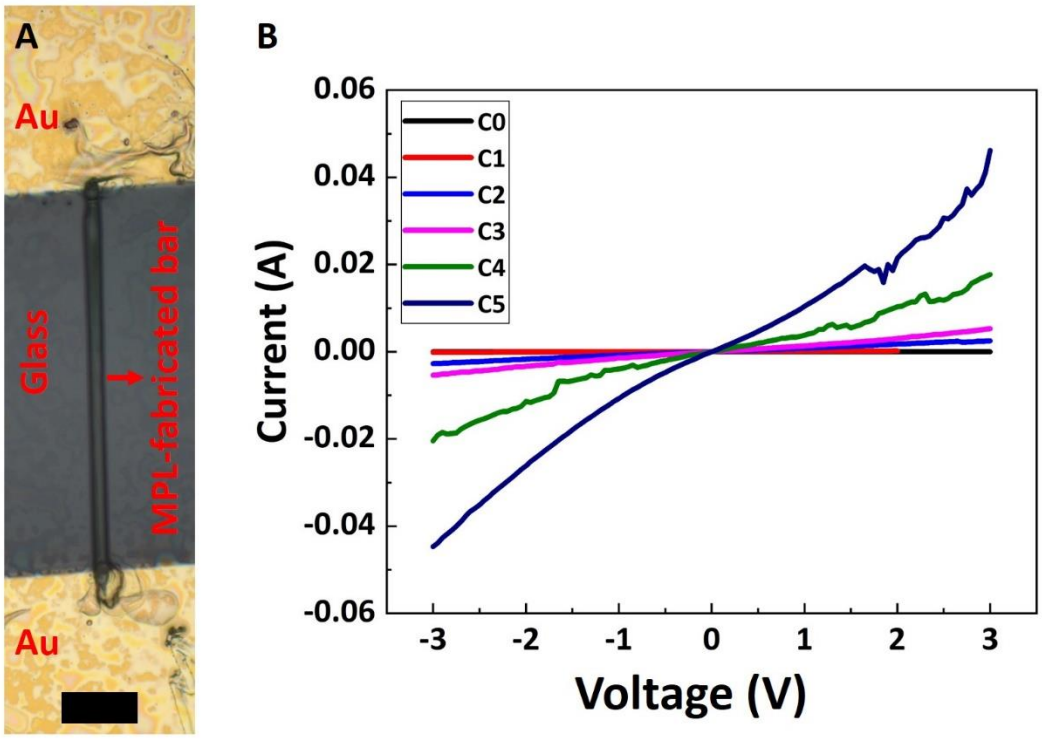

Figure S6. Conductivity measurement: A) MPL-fabricated line on a partially gold-coated coverslip (scale bar: 50 µm). B) I-V curves of lines fabricated with resins with various OS concentrations 0 wt% (C0, black), 0.1 wt% (C1, red), 0.2 wt% (C2, blue), 0.3 wt% (C3, magenta), 0.4 wt% (C4, green), and 0.5 wt% (C5, dark blue). Voltage ranged between -3 V and 3 V, while current was automatically recorded.

Effect of DMSO concentration on Electrical Conductivity

Effect of DMSO concentration on conductivity of MPL-fabricated microstructures was investigated. In the range of MPL-processible DMSO concentration (25-35 wt%), the

conductivity was measured to be $2.8\times10^4 \pm 7\times10^3$, $2.9\times10^4 \pm 4.2\times10^3$, $2.8\times10^4 \pm 2.8\times10^3$, $2.8 \times 10^4 \pm 4.5\times10^3$, and $2.8\times10^4 \pm 4.9\times10^3$ S m^{-1} for resins with DMSO concentration of 25, 27.5, 30, 32.5, and 35 wt%, respectively. As shown, varying DMSO concentration in the resin (containing 0.5 wt% OS) in the range of 25-35 wt% did not significantly change the electrical conductivity of MPL-fabricated microstructures.

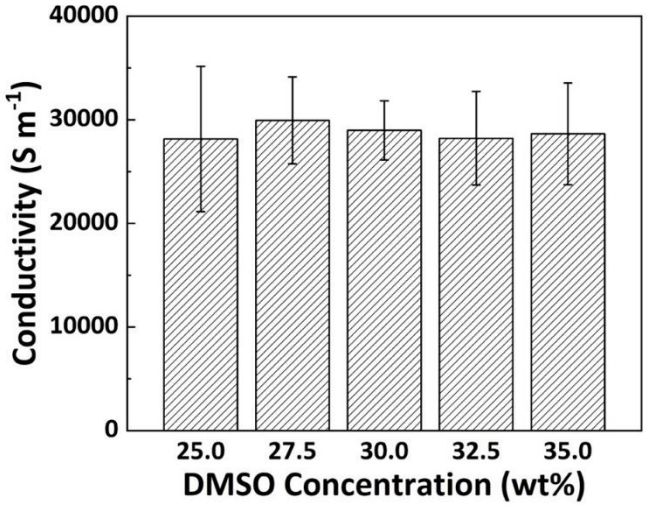

Figure S7. Effect of DMSO concentration in the resin on electrical conductivity. Data shown as mean ± SD, n=4.

Materials Confocal Microscopy (MCM)

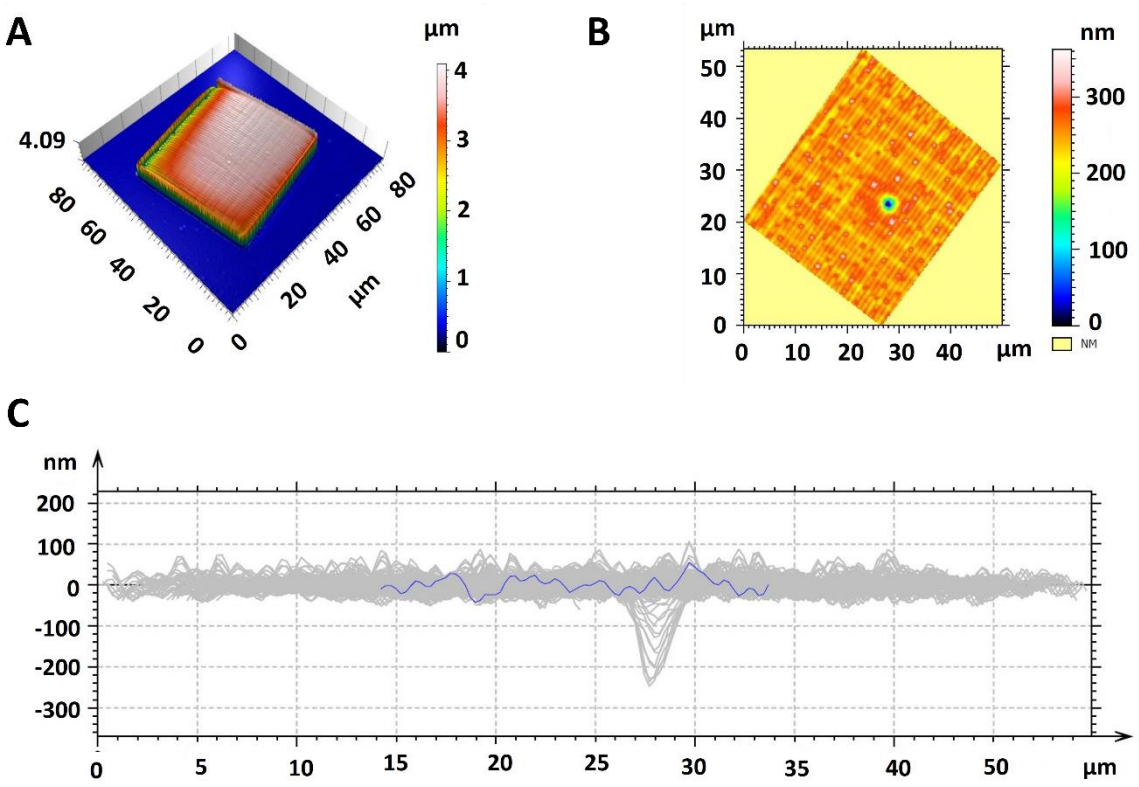

Figure S8. MCM of the MPL-fabricated polymer composite microcube. A)3D view of color-coded height map. B) Color coded surface topography of the cube (area of 50 µm × 50 µm was extracted for roughness measurements), and C) Surface roughness profile.

Table S1. Specific electrical conductivity of MPL-fabricated microstructures in the literature.

Conductive Agent	**Concentration (wt%)**	**Resin**	**Feature size (Line width)**	**Specific conductivity (S m^{-1} $wt\%^{-1}$)**	**Reference**
CNT	0.01	Femtobond 4B	450 nm	7	23
CNT	0.2	Acrylic-thiol	310 nm	2.3×10^{2}	24
Graphene	≈ 0.02	Silicon/Zirconium	≈ 1µm	1.4×10^{-3}	26
EDOT	≈ 20	PEGA	N/A	2×10^{-1}	60
$HAuCl_4$	30	SU-8	800 nm	8.3×10^{5}	21
Ag nanowires	0.4	Thiol-acrylate	200 nm	2.3×10^{2}	20
MWCNT-doped resin + PEDOT:PSS *In situ* self-assembly	0.32	Acrylamide	N/A	1.41×10^{2}	62
MWCNT-doped resin + PEDOT Interpenetration	0.25	PEGA	500 nm	8.9	61
CNT	5	Ormocers b59	N/A	1.94×10^{-7}	25
$HAuCl_4$	≈ 1.87	SU-8	4 µm	9.2×10^{3}	22
$HAuCl_4$	50	PEG-triacry (annealing)	1 µm	4.4×10^{4}	17
Graphene	10	N/A	N/A	9.85E-06	27
$AgNO_3$	7.3	PVP Polyvinylpyrolidone	200 nm	3.9×10^{5}	59
$AgBF_4$	0.2	PVK polyvinylcarbazole	300 nm	1.5×10^{6}	58

Table S2. Length of resistor elements (lines) in the micro-printed circuit board. All lines have thickness and width of 2 µm and 1 µm, respectively. Length of the elements was measured using ZENPro software.

Element	Modeled Length (µm)	Measured length (µm)
a1	180	180.02
a2	155	155.16
a3	130	129.21
a4	70	70.01

Table S3. Dimensions of the microcapacitor. Length, width, and height of the elements were measured using ZENPro software.

Element	Modeled Length (µm)	Measured Length (µm)	Modeled Width (µm)	Measured Width (µm)	Modeled Height (µm)	Measured Height (µm)
Cubic pad	20	20.03	20	20.03	2	2.05
Cable (one side)	430	430.53	1	1.12	2	2.03

Calculation of Specific Capacitance

Specific capacitance (C_{SP}) of the OS-composite microstructures was calculated using the following equation:

$$C_{sp} = \frac{1}{2\Delta V \upsilon m} \int_{V_1}^{V_2} i \, dV \quad \text{(S2)}$$

, where υ is scan rate (0.1 V s^{-1}), A is surface area, m is the mass of the microstructres, and ΔV is the potential sweep window. Mass of the microcapacitors was calculated based on the density of OS-composite resin (ρ= 1.14 pg μm^{-3}).

Laminin incorporation within the microstructures

To investigate the immobilization of laminin within the microstructures, line scans were created at various locations and fluorescent intensity of laminin was measured (**Figures S9A** and **S9B**). The results showed that in LM-OSCMs, the fluorescent intensity was 10345 ± 573 AU with coefficient of variance of 5.5 % (n=14, mean ± SD).

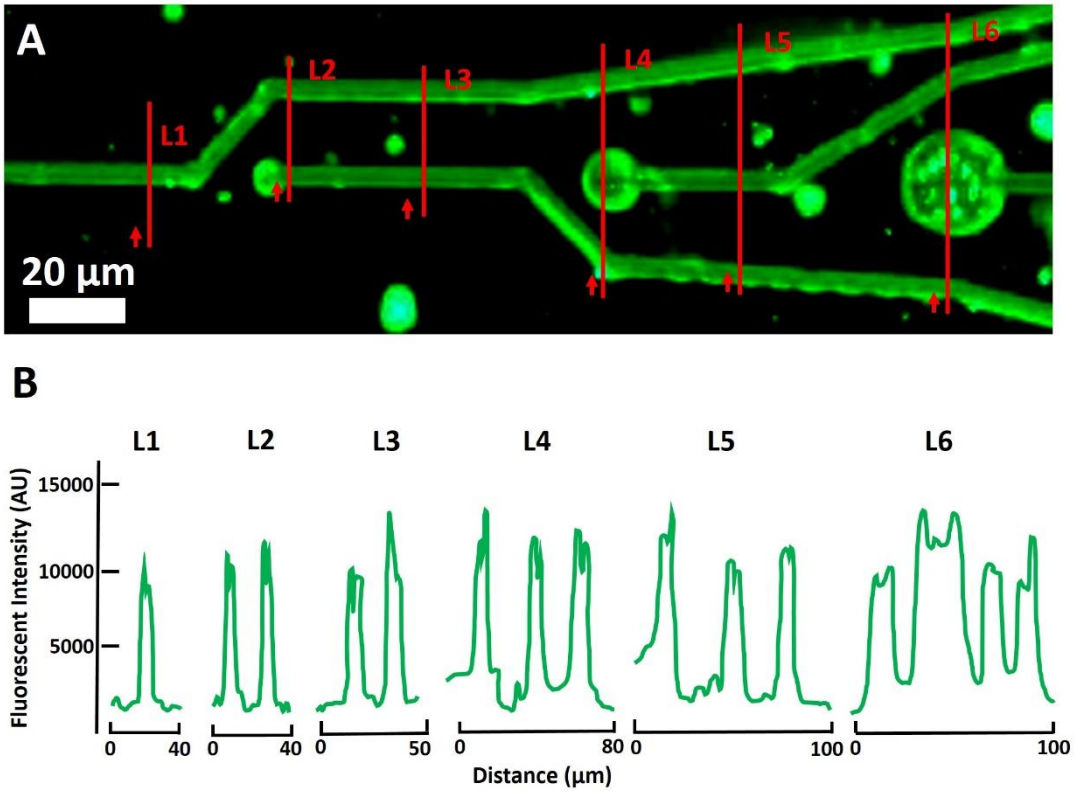

Figure S9. Laminin incorporation within the OS microstructure. A) Fluorescent micrograph of LM-OSCMs after immunohistochemistry (IHC). B) Line intensity scans across (red lines) as indicated in IHC image.

Swelling, mass loss, and impedance change over time

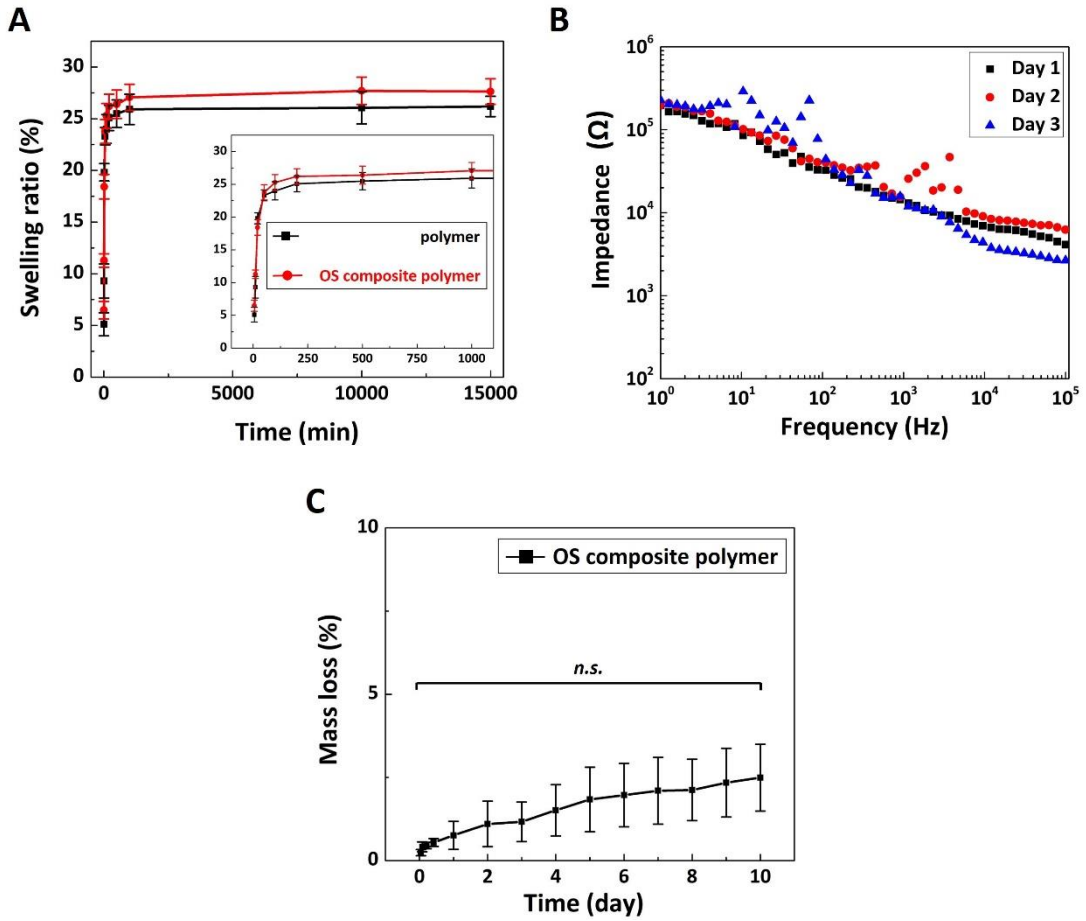

Figure S10. Swelling, mass loss and impedance change over time. A) Swelling ratio (%) with respect to time for polymer and OS-polymer composite structures (n=5, mean ± SD). B) Impedance of the MPL-fabricated microelectrode site (diameter: 80 µm) over 3 days (day 1, 2, and 3 are shown by black square, red circle, and blue triangle, respectively. C) Mass loss (%) of OS composite structures over 10 days. Data shown as mean ± SD, n=5, n.s. represents no significance.

Calculation of Charge Storage Capacity:

The charge storage capacity (Q) of the OS-composite microstructures was calculated based on the following equation:

$$Q = \frac{1}{\upsilon A}\int_{V_1}^{V_2} i\, dV \quad \text{(S3)}$$

, where υ is scan rate (0.1 V s^{-1}), A is surface area, and ΔV is the potential window ($\Delta V = 1.2\ V$).

Specific Capacitance of OS-Composite Microelectrodes

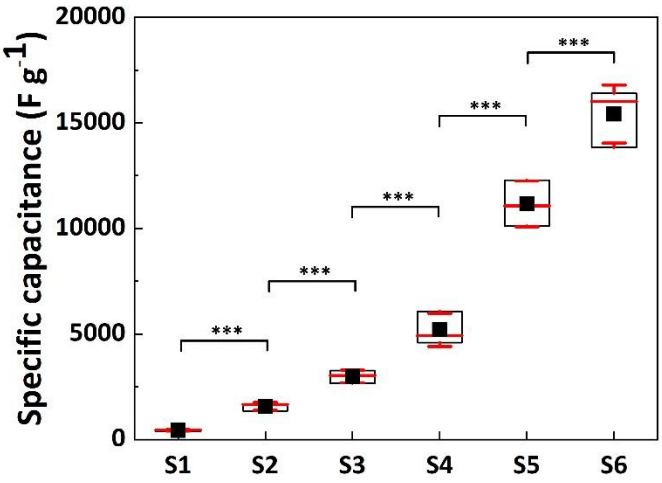

Figure S11. Specific capacitance of OS-composite sites. Data is represented in a box graph where the black squares, red lines, and red whiskers demonstrate mean, median, and standard deviation, respectively (n=3).

GOx-OS composite resin and electrical properties of GOx-OS composite microelectrodes

As shown in **Figure S12A**, addition of GOx to OS resin (with a light blue color due to presence of OS), gives a yellow hue to the GOx-OS composite resin. Impedance spectrum (**Figure S12B)** and cyclic voltammetry (**Figure S12C**) were compared between OS composite and GOx-OS composite microelectrode sites (GOx-OSCMs) with diameter of 80 µm.

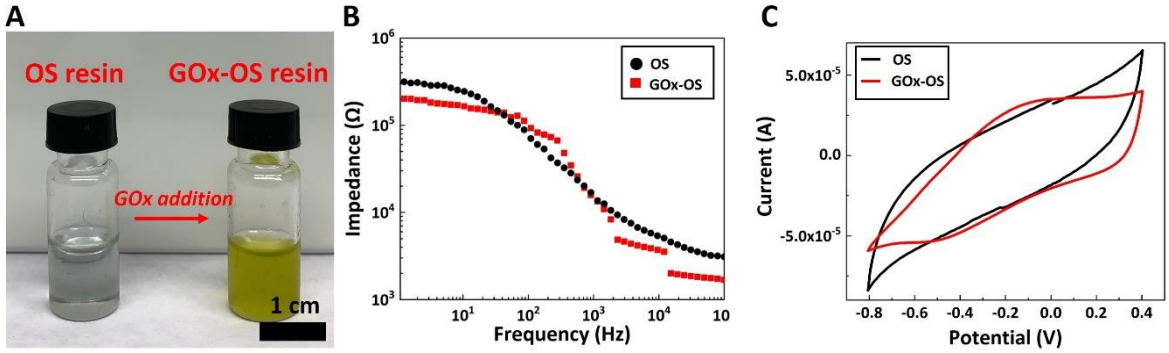

Figure S12. GOx-OS composite resin and electrical properties of the microelectrode: A) Addition of GOx to the OS resin. B) Impedance spectrum of OSCM microelectrode cites (black circles) and GOx-OSCM microelectrode cites (red square). C) CV curves of OSCM microelectrode cites (black curve) and GOx-OSCM microelectrode cites (red curve).

Glucose detection in deoxygenated buffer solution

To validate the oxygen independent redox reaction and the OS mediation at bias potential +0.3V, the glucose detection was performed at both bias potentials of +0.7 and +0.3 V in a deoxygenated PBS. Briefly, an amperometric experiment was performed an amperometric cell containing 20 ml PBS (1X, pH= 7.4, T=37^{o}C) after deoxygenation by pure N_2 for 1hr. An N_2 environment was kept in the cell by blowing N_2 continuously during the experiment. BioStat^{TM} (ESA Biosciences, Inc.) was used to record the current response at

polarization potential of +0.3 V and +0.7 V vs. Ag/AgCl. A magnetic stirrer provided the convective transport for the amperometric experiments after the background current was allowed to decay to a steady state. Then 0.2 mM glucose was added to the cells and the amperometric response was recorded. As shown in Figure S13, while the GOx-OSCM biosensor did not generate any current response at +0.7 V due to deoxygenation, glucose detection was achieved at potential +0.3 V, confirming OS mediated detection.

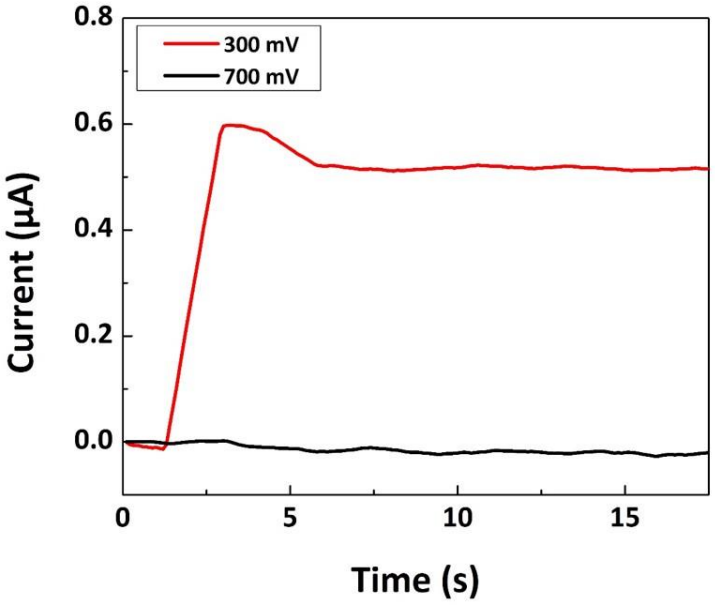

Figure S13. Amperometric glucose detection in a deoxygenated PBS by N_2. Red and black curve show current response upon addition of glucose concentration 0.2 mM at bias potentials or +0.3 mV and +0.7 mV, respectively.

Table S4. Sensitivity of the developed glucose biosensors.

Material	Method	Sensitivity ($\mu A\ cm^{-2}\ mM^{-1}$)	Reference
CP PEDOT:PSS nanofibers	Physical entrapment	6.4	78
CP PEDOT:PSS nanofibers	Physical entrapment	9.2	78
CP PEDOT	Physical entrapment	12.4	86
CP PEDOT film	Physical entrapment	2.7	87
CP Ppy / propylic acid	Covalent attachment	13.4	88
CP PEDOT	Physical entrapment	14.1	94
CP PEDOT:PSS	Physical entrapment	6.43	92
CNT	Covalent attachment	20.6	89
CNT	Covalent attachment	11.3	90
CNT	Covalent attachment	47.8	99
CNT	Physical entrapment	91	93
Gold Au nanoparticles	Covalent attachment	8.8	95
Gold Chitosan – Au nanoparticles	Covalent attachment	69.3	96
Gold Au nano particle	Covalent attachment	5.7	97
Gold Au nano particle	Covalent attachment	3.8	98

Preparation of GOx-OSCM and GOx-OS biosensors and amperometric measurements

As described, GOx-OSCM biosensors (encapsulated enzyme) were fabricated using the MPL process from a homogeneous resin containing 0.3 mM GOx and 0.5%wt OS. GOx-OS biosensors (entrapped enzyme) were fabricated on gold electrodes. A solution containing 0.02 M OS monomer, 0.2 M PSS, and 0.3 mM GOx was prepared in DI water. Electrochemical polymerization was carried out by electrodeposition of GOx-OS galavanistatically on gold electrodes using Autolab PGSTAT 302N (Metrohm Autolab, Netherlands) in two-electrode

configuration at a charge density of 150 mC cm $^{-2}$. After electropolymerization, the GOx-OS electrodes were rinsed several times with distilled water to remove any loosely bound enzyme and any remaining OS monomer. Figures S14A and S14B show amperometric current response for GOx-OSCM biosensors and GOx-OS biosensors, respectively at a pre-set polarization potential of + 0.3 V vs. Ag/AgCl upon injection of increasing glucose concentration from 0.1 mM to 3 mM in phosphate buffered saline (PBS, pH= 7.4, T= 37ºC). The GOx-OSCM biosensor exhibited ~50-fold higher sensitivity compared to GOx-OS biosensor.

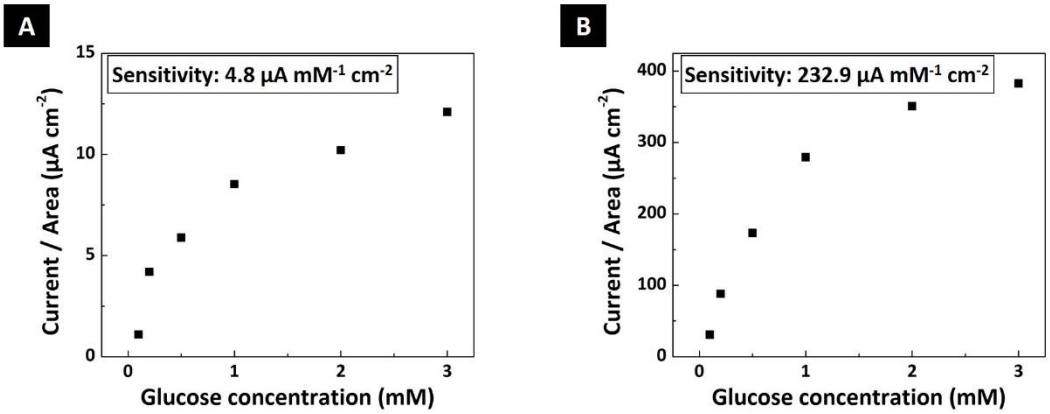

Figure S14. Response curve of biosensors to addition of glucose concentrations : (A) GOx-OS biosensor (entrapped enzyme), (B) GOx-OSCM biosensor (encapsulated enzyme).

Femtosecond Laser Specifications:

Two-photon polymerization laser (Mai Tai™ DeepSee, MTEV HP 1040 S, Spectra Physics) was utilized to fabricate microstructures.

The spot size of the laser (θ) was calculated to be 1.5 µm based on the following formula:

$$\theta = 1.22 \frac{\lambda}{N.A.} \quad \text{(S4)}$$

, where λ is the laser wavelength (780 nm), and N.A. is the numerical aperture (0.65) of the 40X objective (Plan N, OLYMPUS).

Energy of pulse (E) was measured to be 2.5×10^{-10} J from this equation:

$$E = \frac{p}{f} \quad \text{(S5)}$$

, where p is average laser power (20 mW) and f is repetition rate of the laser beam (80 MHz).

Peak power (PP) was calculated to be 2.5 W from the following equation:

$$PP = \frac{E}{\omega} \quad \text{(S6)}$$

, where ω is laser pulse width (100 fs).

Energy density (σ) of the laser beam was measured to be 0.014 J cm^{-2} using the following formula:

$$\sigma = \frac{E}{A} \quad \text{(S7)}$$

, where A is the area of the spot size ($\pi\theta^2/4$).

Power density (ρ) of the laser beam was calculated to be 141.54 MW cm^{-2} using the following equation:

$$\rho = \frac{PP}{A} \quad \text{(S8)}$$

To calculate the exposure time of resin to laser beam (t) was calculated to be 0.03 s by using the following equation:

$$t = \frac{\theta}{v} \quad \text{(S9)}$$

, where v is fabrication velocity (50 μm s^{-1}), and θ is the spot size (1.5 μm).

Biocompatibility assessment

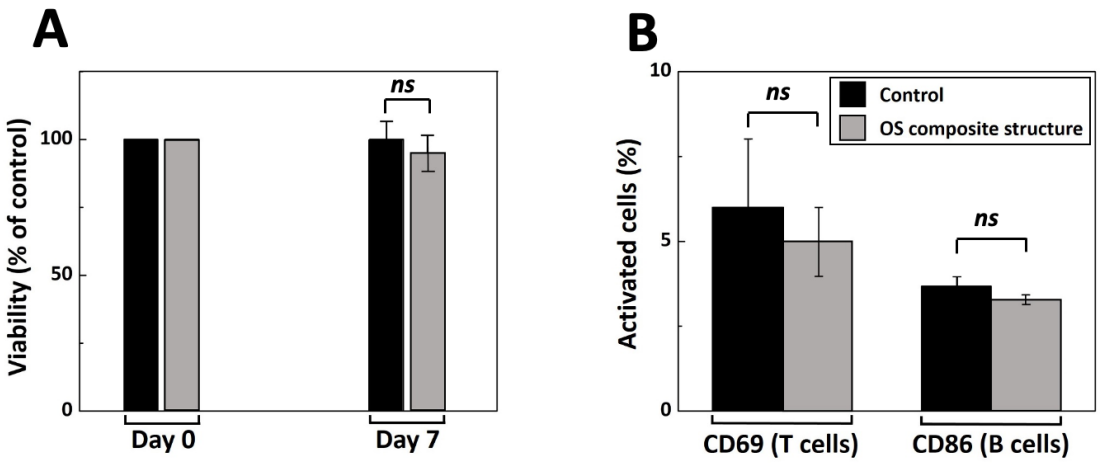

Figure S15. Biocompatibility assessment of OS composite structures on splenic immune cells after 7 days. Total splenic cells from a mouse were cultured for 7 days on OSCM or control structures. A) Viability (normalized with respect to control) comparison between OS composite structures and control on day 0 and day 7. B). The percentage of activated splenic T cells (assessed using CD69) and B cells (assessed using CD86) after 7 days of culture on OSCM or control structures, as assessed using flow cytometry. OS composite structure and control (without structure) are shown in black and grey bars, respectively. Data s shown as mean ± SD , n=3, ns represents no significance . The initial cell count was 5000000 cell /ml for all samples, therefore there are no error bars for A at day 0.

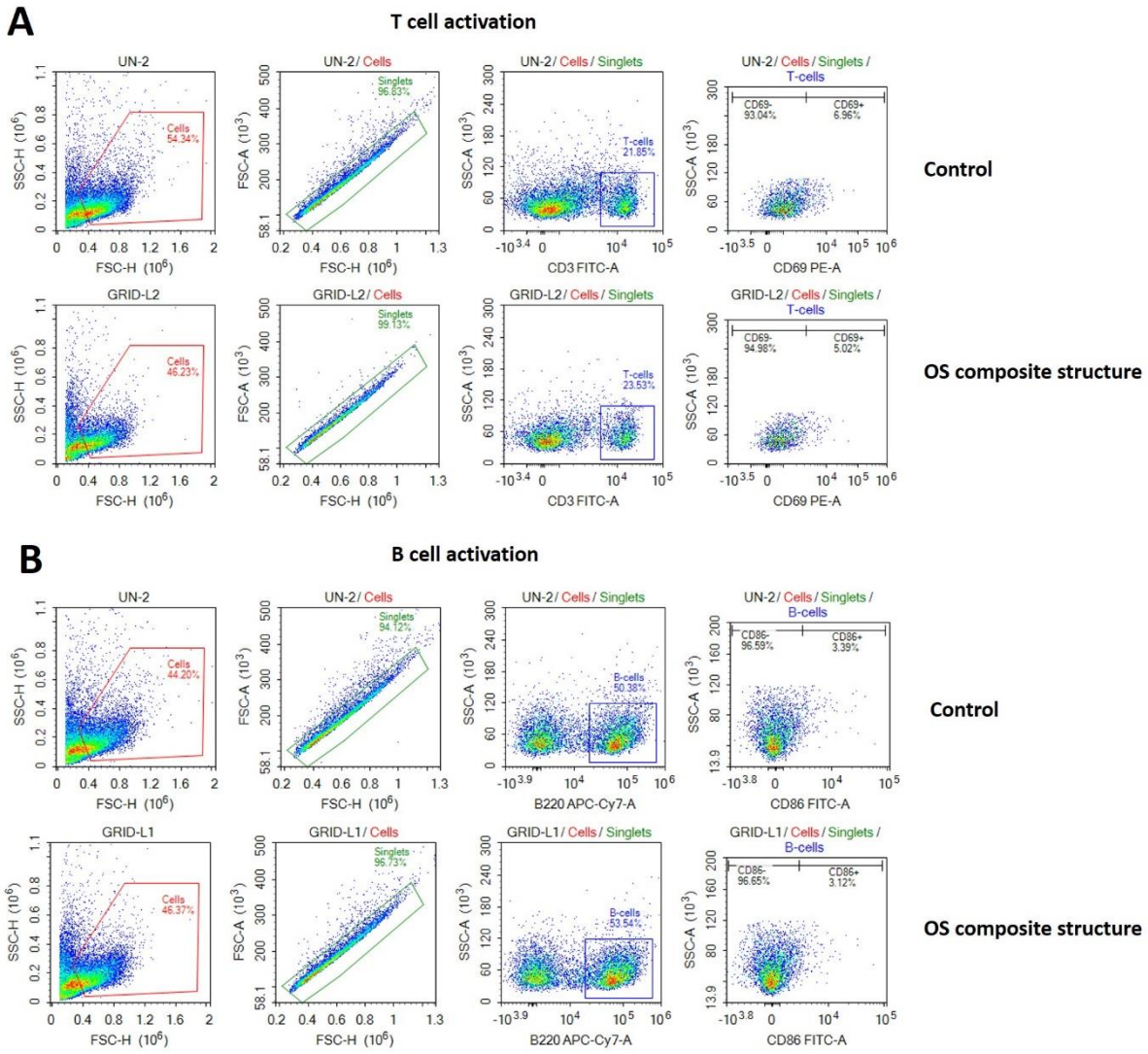

Figure S16. Flow cytometry analysis of splenic lymphocytes for biocompatibility assessment. Total splenic cells from a mouse were cultured for 7 days on OSCM or control structures. After gating splenic cells from a healthy mouse and using a side scatter (SSC) vs forward scatter (FSC) plot to exclude debris, doublets and clumps, single cells were gated using FSC-A vs FSC-H plot. The singlets were then characterized by fluorophore conjugated antibodies. T-cells are identified by positive staining for the T-cell marker CD3, and the gated T-cells were explored for the surface expression of CD69 which is a marker for activated T-cells (A). Similarly, B-cells were identified by positive staining for B220 and the gated B-cells were analyzed for the expression of CD86, which is a marker for activated B-cells (B). Note: no activating triggers were deliberately added to these cultures; the intent was to see if the fabricated structures can themselves activate the lymphocytes.